

LA-UR-95- 3057

Title:

ELEVATED TEMPERATURE STRESS-STRAIN  
BEHAVIOR OF BERYLLIUM POWDER PRODUCT

Author(s):

STEPHEN P. ABLEN, MST-6  
ROBERT D. FIELD, MST-6  
MARTIN MATAYA, SAFE SITES IF COLORADO, RFETS

Submitted to:

SECOND IEA INTERNATIONAL WORKSHOP ON  
BERYLLIUM TECHNOLOGY FOR FUSION, JACKSON  
HOLE, SEPTEMBER 6-8, 1995

MASTER

DISTRIBUTION OF THIS DOCUMENT IS UNLIMITED *at*



**Los Alamos**  
NATIONAL LABORATORY

ELEVATED TEMPERATURE STRESS STRAIN BEHAVIOR OF  
BERYLLIUM POWDER PRODUCT

by

S.P. Abeln\*  
M.C. Mataya\*\*  
R. Field\*

\* Los Alamos National Laboratory

\*\* Safe Sites of Colorado, Rocky Flats Environmental Technology Site

**DISCLAIMER**

This report was prepared as an account of work sponsored by an agency of the United States Government. Neither the United States Government nor any agency thereof, nor any of their employees, makes any warranty, express or implied, or assumes any legal liability or responsibility for the accuracy, completeness, or usefulness of any information, apparatus, product, or process disclosed, or represents that its use would not infringe privately owned rights. Reference herein to any specific commercial product, process, or service by trade name, trademark, manufacturer, or otherwise does not necessarily constitute or imply its endorsement, recommendation, or favoring by the United States Government or any agency thereof. The views and opinions of authors expressed herein do not necessarily state or reflect those of the United States Government or any agency thereof.

## **DISCLAIMER**

**Portions of this document may be illegible in electronic image products. Images are produced from the best available original document.**

## ACKNOWLEDGMENTS

The authors wish to thank Don Kaczynski of Brush Wellman Inc for supplying material and Donna Rune' for her never ending help in test set-up and data collection.

## ABSTRACT

Several grades of beryllium powder product were tested under isothermal conditions in compression over a temperature range of room temperature to 1000°C and a strain rate range from 0.001 s<sup>-1</sup> to 1 s<sup>-1</sup>. Samples were compressed to a total strain of 1 (64% reduction in height). It is shown that all the grades are strain rate sensitive and that strain rate sensitivity increases with temperature. Yield points were exhibited by some grades up to a temperature of 500°C, and appeared to be primarily dependent on prior thermal history which determined the availability of mobile dislocations. Serrated flow in the form of stress drops was seen in all the materials tested and was most pronounced at 500°C. The appearance and magnitude of the stress drops were dependent on accumulated strain, strain rate, sample orientation, and composition. The flow stress and shape of the flow curves differed significantly from grade to grade due to variations in alloy content, the size and distribution of BeO particles, aging precipitates, and grain size. The ductile-brittle transition temperature (DBTT) was determined for each grade of material and shown to be dependent on composition and thermal treatment. Structure/property relationships are discussed using processing history, microscopy (light & transmission), and property data.

## INTRODUCTION

Figure-1 shows the variation of ultimate tensile strength and elongation for a wrought, fine grained, high purity beryllium product over a temperature range from 300°C to 1000°C (the strain rate was not reported).<sup>1</sup> The smooth curves demonstrate that this high purity material is well behaved and predictable.

Conventional beryllium powder product is considerably less pure and its properties are affected by processing and impurity content.

Some examples of reported discrepancies from ideally simple behavior include: yield points, serrated flow, ductility minimums, superplastic behavior, and anisotropy associated with texture.

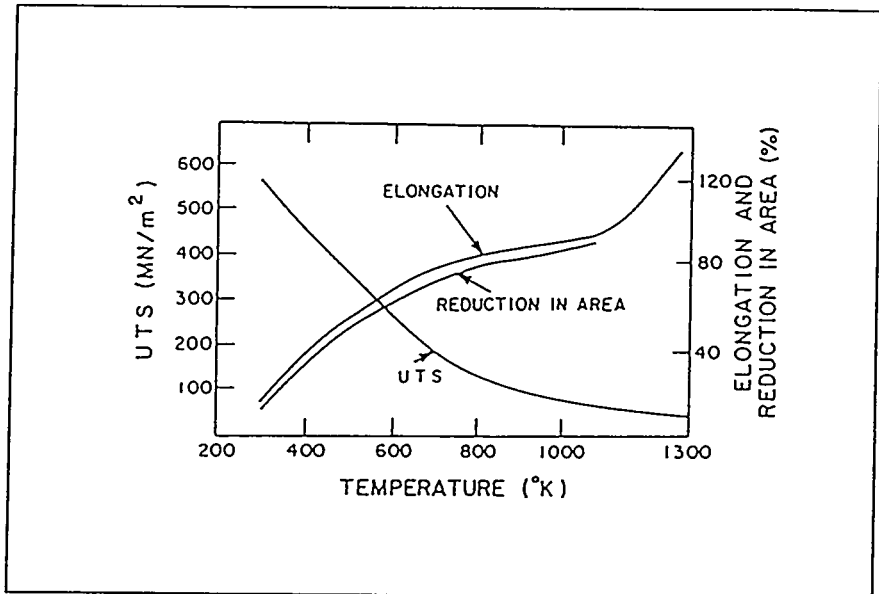


Figure 1 Temperature dependence of the mechanical properties for a fine grained, high purity wrought product.

Metal flow is typically thermally activated and therefore temperature and strain rate sensitive. Thus, the characterization of material deformation at high temperature must include the stress-strain behavior as a function of temperature and strain rate. The majority of data in the literature pertains only to specific operational requirements, and is therefore limited.

The objective of this study is to establish a high temperature stress-strain data-base for beryllium powder product and provide structure/property information. The data-base spans a range of beryllium microalloyed materials made to different specifications to provide insight into the effects of chemistry, processing history and starting microstructure on high temperature stress-strain behavior. The data-base goes beyond normal structural performance requirements (in both temperature and strain rate) and provides information to the metallurgist interested in the shaping of beryllium components via various forming and consolidation operations.

## BACKGROUND (Structure/Properties)

Impurities or microalloy content play a major role in the stress-strain behavior of beryllium. The principle impurities that affect stress-strain behavior are BeO, Al, and Fe, and are introduced during the manufacturing process. Several variables, such as, consolidation technique, impurity concentration/solubility, and heat treat can affect the distribution and morphology of these elements. The origin and microstructural evolution of these impurities during processing, and their effect on elevated temperature properties, are discussed below.

### BeO

The oxide, BeO, forms on all exposed surfaces of powder during the comminution process. Oxide levels in powder product, compared to cast and wrought product, are therefore inherently higher due to the high total surface area of the combined powder particles. The oxide layer is altered during the consolidation process to produce discrete particles.

Webster et al<sup>2</sup> found BeO at two locations in hot pressed beryllium block; 1) along the grain boundaries, and 2) at isolated clusters within the grain. Oxide growth at these two locations was observed to differ. The growth of BeO at high angle grain boundaries was found to be accelerated by higher concentrations of Al, Mg, and Si, and higher consolidation temperatures. The growth of BeO within the matrix was found to be negligible, regardless of purity or processing temperature. The discrepancy between oxide growth rate within the grain boundaries and matrix demonstrates that the low melting impurities (Al, Si, Mg), which segregate preferentially to the grain boundaries, are the principle controlling factors for grain boundary oxide distribution and morphology. The BeO particles within the matrix are unaffected because the low melting impurities are not soluble within the matrix.

The presence of liquid phases at particle/grain boundaries, which can form at relatively low temperatures if impurities are present, can further enhance diffusion of Be and oxygen causing rapid coarsening of BeO. In addition to the low melting phases, the pressure-temperature cycle during consolidation was also found to influence BeO size and distribution.

Webster et al<sup>2</sup> found that when pressure was applied early in the pressing cycle, the extent of oxide coarsening was reduced. This apparently results from different diffusivities between free surfaces in the compact and particles which are in contact or bonded.

The relationship between BeO size and distribution, and consolidation temperature implies that the distribution of BeO can be controlled through appropriate processing. In fact, variations in oxide morphology and distribution have been observed with different consolidation techniques<sup>3</sup>. The two principle consolidation techniques utilized for beryllium powder product are hot isostatic pressing (HIP) and vacuum hot pressing (VHP). HIP employs higher pressures while VHP pressures are limited by die material constraints. The lower pressure associated with VHP

requires higher consolidation temperatures to achieve full density. Typical consolidation parameters for HIP and VHP are as follows:

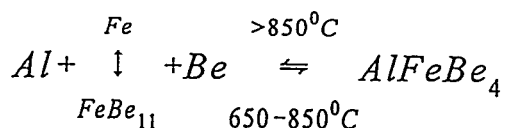
- HIP- 1000°C/15ksi/3 hrs
- VHP- 1050-1150°C/2ksi/36 hrs

The difference in oxide size and distribution between the same material consolidated by these two different techniques is primarily in the grain boundary because matrix BeO is not affected by consolidation. The HIP process typically produces a fine (0.05-0.1µm) uniform dispersion along the grain boundaries and the VHP process a coarsened (0.1-0.50µm), relatively heterogeneous dispersion.<sup>3</sup>

The effect of BeO on properties is complex. At elevated temperatures, BeO behaves similarly to a fine dispersoid in dispersion strengthened materials in that it inhibits grain growth and stabilizes the microstructure. At elevated temperatures, stable grain size, improves creep properties. At lower temperatures, BeO particles act as stress concentrators which can initiate cracks under certain conditions.

#### Al-Fe

It has been established that control of the levels of certain microalloy elements, combined with proper heat treating cycles, can dramatically change the mechanical properties of beryllium, particularly at elevated temperature.<sup>4</sup> The principle microalloy elements have been identified as Fe and Al, which together interact synergistically. Their interaction can best be described as follows:<sup>4</sup>



The reaction states that at temperatures greater than 850°C, the ternary compound dissolves leaving free Al at the grain boundaries and Fe in the matrix. The Fe is present in solid solution or the binary precipitate FeBe<sub>11</sub>. At temperatures between 650-850°C the ternary precipitate forms at the grain boundaries. Formation of the ternary requires diffusion of Fe out of the matrix and into the grain boundary, depleting Fe from the matrix.

One of the important aspects of this reaction on the high temperature properties relates to the free Al. Excess free Al at the grain boundaries accounts for observed high temperature ductility minimums or hot shortness in beryllium. Aluminum melts at 660°C and there is a Be-Al eutectic at 645°C. Therefore, material containing excess Al would be expected to fail intergranularly under stress above approximately 650°C. In fact intergranular failure associated with free Al has been observed as low as 350°C<sup>5</sup>. The lower limit of free Al at which intergranular failure will occur has been determined to be 200ppm<sup>4</sup>. Therefore it is important to control the relative

proportions of the Al and Fe, so that sufficient Fe is present to combine with all of the free Al. The atomic weight of Fe is approximately twice that of Al so that the proper proportion is at least twice as much Fe by weight to account for all the Al.

The other important aspect of the above reaction is the quantity and form of Fe within the matrix. Matrix Fe is dependent on the total Fe content and any depletion which may have occurred due to migration to the grain boundaries during heat treatment. The Fe in the matrix appears either in solid solution or as a precipitate ( $\text{FeBe}_{11}$ ). The precipitate forms when the solid solubility is exceeded during heat treat. Precipitation of  $\text{FeBe}_{11}$  is favored below  $650^\circ\text{C}$ . The solubility of Fe in beryllium has been shown by Myers and Smugeresky<sup>6</sup> to depend on the presence of Al. The solubility of Fe in high purity Be is about 1000ppm (0.1wt%) at  $500^\circ\text{C}$  and about 10,000ppm (1wt%) at  $850^\circ\text{C}$ . In the presence of Al the solubility drops to about 600ppm (0.06wt%) below  $850^\circ\text{C}$ .

Beryllium is strengthened by Fe in solid solution. Floyd<sup>7</sup> reported a 2.3 psi increase in room temperature yield stress per ppm of Fe for solutionized beryllium. Aged conditions which precipitate  $\text{FeBe}_{11}$  also showed strength increases, but were more difficult to define quantitatively. Floyd attributed this to two mechanisms 1)softening by removing Fe from solution (forming  $\text{AlFeBe}_4$  and  $\text{FeBe}_{11}$ ) and 2)hardening by precipitation ( $\text{FeBe}_{11}$ ).

Two yield phenomena have been related to the solute atoms or precipitation reactions discussed above, yield points and serrated flow. Yield points have been seen at room temperature and elevated temperatures. Serrated flow is a high temperature phenomenon which is strain rate dependent.

Yield points have been attributed to precipitate pinning. Floyd<sup>7</sup> suggested that yield points were due to  $\text{AlFeBe}_4$  precipitates while Stonehouse<sup>3</sup> indicated that  $\text{FeBe}_{11}$  was the source. In either case, the precipitates are thought to pin dislocations, reducing the number of glissile dislocations sufficiently to require new dislocations to be generated at a higher stress level. Yield points have not been observed above  $650^\circ\text{C}$ <sup>3</sup>.

Serrated yielding has been observed in a number of different studies<sup>8-10</sup>. The most detailed study by Weisz, et al<sup>10</sup> showed serrated yielding occurred between  $350$  and  $550^\circ\text{C}$  in cast-extruded metal in the solutionized condition. They attributed the serrated yielding to Fe in solution for the following reasons:

- Plastic deformation was required prior to the occurrence of the serrations, indicating a probable substitutional element which requires the enhanced diffusion offered by a vacancy rich deformed lattice.
- Serrated yielding was eliminated by heat treatment for 100 hrs at  $650^\circ\text{C}$  which precipitated  $\text{FeBe}_{11}$ .

### Grain Size

Grain size in powder product beryllium is controlled by the input powder particle size and the

consolidation temperature. The smaller the powder particle size and the lower the consolidation temperature the smaller the final grain size will be. This is advantageous from the standpoint that beryllium has been shown to follow the Hall-Petch relationship, where strength is proportional to the inverse square root of the grain size and therefore finer grain size results in improved strength. A Hall-Petch plot for high purity beryllium block is shown in figure-2.<sup>11</sup> Note that a reduction in grain size from 10 $\mu$  to 5 $\mu$  results in an approximate increase in Y.S. of 130 Mpa. As grain size is reduced further even

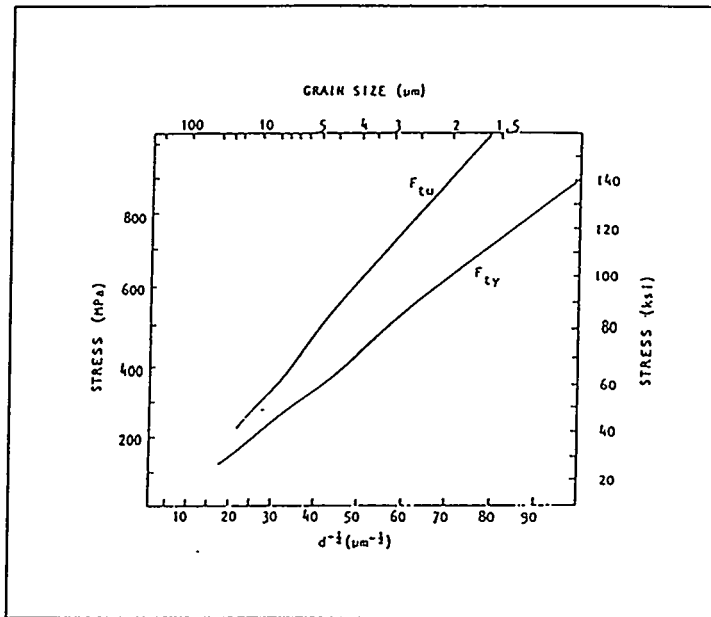


Figure 2 Hall-Petch plot for high purity beryllium block.

greater increases in strength are realized. For example, a reduction in grain size from 5 $\mu$  to 3 $\mu$  results in an approximate increase in Y.S. of 160 Mpa. In addition, finer, more isotropic grain size and distribution have led to improved ductility. The improved ductility is attributed to greater slip compatibility within the matrix, reducing the stress concentrations and crack propagation associated with anisotropic orientations. However, reducing the powder particle size also increases the BeO content which in turn reduces ductility. Therefore there is generally a compromise particle size/grain size for optimum strength and ductility.

### Texture

A mild texture is generally found in hot-pressed beryllium. The texture not only relates to nonisotropic consolidation techniques (VHP) but also to the shape of the powder particles. Due to the anisotropic nature of the beryllium single crystal, particles are fractured along basal planes during comminution which leads to a flat-like powder particle. These particles tend to align themselves during die or can filling. Thus, mild textures are formed even under isotropic consolidation conditions. Basal textures of vacuum hot pressed beryllium in the pressing direction are typically 1.3 to 1.8 random<sup>9</sup>. The various textures have little effect on the yield or ultimate strengths, but significantly affect ductility. Typical elongations can vary by a factor of two, with the longitudinal orientation (parallel to the pressing direction) showing lower elongations and transverse (perpendicular to the pressing direction) exhibiting higher elongations. This appears to be due to the higher population of basal planes perpendicular to the stress axis in the longitudinal orientation, and their propensity to generate and propagate cleavage cracks.

# EXPERIMENTAL APPROACH

## Material

Table-1 shows the matrix of materials evaluated with their associated microalloy concentrations, tensile properties, grain size, and heat treat condition (when known).

Table-1

MATERIAL	CHEMISTRY				PROPERTIES				
	Si	Al	Fe	BeO	YS	UTS	EL%	GS( $\mu$ )	HT
	WEIGHT %				(ksi)	(ksi)			
P31664	0.025	0.038	0.09	0.72	35	54	6T,3L	11	OA
S200F(spec)	0.06	0.1	0.13	1.5	35	47	2	<20	
S200E	0.03	0.03	0.06	1.6	38	56T,52L	2T,1L	9.3	NO
RM253939	0.034	0.016	0.058	0.79	41	63	6T,3L	9.4	OA
S65(spec)	0.06	0.06	0.08	1	30	42	3	<15	
S65(cert)	0.02	0.02	0.09	0.6	40	52	7T,3L	12.2	
S65(cert)	0.02	0.03	0.06	0.6	34	54	6T,4L	10.3	
CIP-HIP-1	0.004	0.004	0.018	1.09	35 <sup>1</sup>	50 <sup>1</sup>	3 <sup>1</sup>	9	NO
I250	0.02	0.07	0.07	1.9	76	83	4.3	5	SR
1400	0.05	0.03	0.18	6.2	NR	89T,50L	NR	4.5	NO

1- SPECIFICATION REQUIREMENT

SR- STRESS RELIEF

OA- OVERAGE

NR- NOT REPORTED

NO- NO POST CONSOLIDATION HEAT TREATMENT

Two heat treatments commonly given to beryllium product are stress relief and over aging. The stress relief consists of heating at 1450°F (788°C) for a hold time of one hour per inch of thickness followed by a slow cool of 50°F/hour. The overage heat treatment is a multi step process:

- 1)heat to 871°C and hold for 4 hours
- 2)cool to 746°C and hold for 12 hours
- 3)cool to 728°C and hold for 12 hours

- 4) cool to 717°C and hold for 12 hours
- 5) cool to 704°C and hold for 4 hours
- 6) cool to 690°C and hold for 4 hours
- 7) remove from furnace and air cool

note: cool down time may be included in the hold time in each step.

The extensive times at temperature for the overage heat treatment are to ensure sufficient diffusion of Fe to the grain boundaries.

This range of material types provides a wide contrast in microstructure and properties for study. The following is a brief description of each material.

P31664 is a DOE production specification consolidated by VHP and the most commonly used weldable grade of beryllium. The Al/Fe ratio is controlled and the material is overaged to tie up the Al in the grain boundaries as the ternary  $\text{AlFeBe}_4$ . The significance of the heat treat, in addition to tying up the free Al, is that it reduces the matrix Fe to approximately 0.018%.

S200E is an older commercial grade of beryllium which utilizes attritioned powder and is consolidated by vacuum hot pressing (VHP). This particular lot was HIP'ed after VHP, probably to achieve full density.

RM253939 is a DOE production specification for high strength and weldable beryllium. The powder is made by impact grinding and consolidation is by HIP. The Al/Fe ratio is controlled and the material is overaged similarly to the P31664 grade. As a result of heat treat, the matrix Fe is reduced to approximately 0.024%. The higher matrix Fe and smaller grain size of this grade results in a higher yield strength when compared to P31664.

CIP-HIP-1 is a high purity grade derived from electrolytic flake. The powder is made by impact grinding and is hot isostatically pressed. There is little need to heat treat this material due to the high purity.

I250 is a new grade of beryllium which achieves higher strength levels and still maintains ductility above 3%. The powder is made by impact grinding and is consolidated by HIP. The grain size is much smaller than the previously discussed grades and the BeO and Fe level increases are kept to a minimum.

I400 is an instrument grade made from ball milled powder and is designed to provide a high micro-yield strength. Contaminate levels are higher than conventional structural grades. This material was VHP'ed.

#### Microstructural Characterization

Light microscopy was used to evaluate grain size and in some cases oxide distribution. The specimens were polished and examined under polarized light. Transmission electron microscopy

(TEM) was used to characterize dislocation content, BeO distribution, and precipitation. Microstructure and prior processing history are used to evaluate properties.

### Mechanical testing

Cylindrical compression samples (figure-3), 12.7mm diameter (.5") by 19.05 mm high (.75"), were machined from each billet with specimen axis parallel to either the billet axis (referred to as the longitudinal direction) or the billet radius (transverse). The end faces were recessed to form a lubricant well, an effective technique for constraining lubricant to the sliding face during compression. High temperature (>300°C) specimens had cylindrical wells and low temperature specimens round lubricant wells with blended radii to minimize stress concentrations. A consistent finish machining schedule of 10-5-2-2 (in thousandths of an inch) was utilized to minimize any effects of machining damage.

The hot compression tests were performed on a computerized 250 KN servo-hydraulic testing machine (manufactured by MTS, Inc.) configured with a specialized hot zone as shown in figure-4. The compression load train consists of Astroloy compression rams fitted with silicon nitride compression platens lapped to 8 RMS surface finish with opposite faces parallel to within 0.0127-mm over a 69.85-mm diameter. The platens are held in place on the rams using waspalloy clamps and bolts. The rams are partially hollow and filled with fiberfax insulation to reduce heat loss and decrease heat-up time. The rams are seated in stainless steel water cooled grips which protect the system load cell and actuator.

The heat source is comprised of a three zone Model #2961 (Applied Test Systems Inc.) clamshell resistance furnace capable of temperatures up to 1200°C. The three zones are controlled independently. The center of the furnace is aligned with the top of the bottom platen where the test specimen is placed and heated to temperature. There is also a quartz observation window to view the test. Thermocouples placed in the upper and lower platens as well as touching the sample are used to monitor temperature. Temperature of the dies and specimen are typically

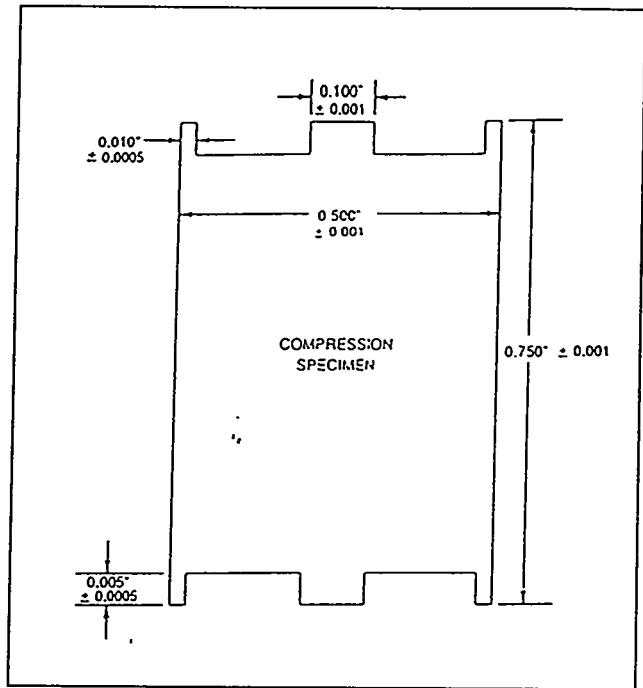


Figure 3 Schematic of compression specimen

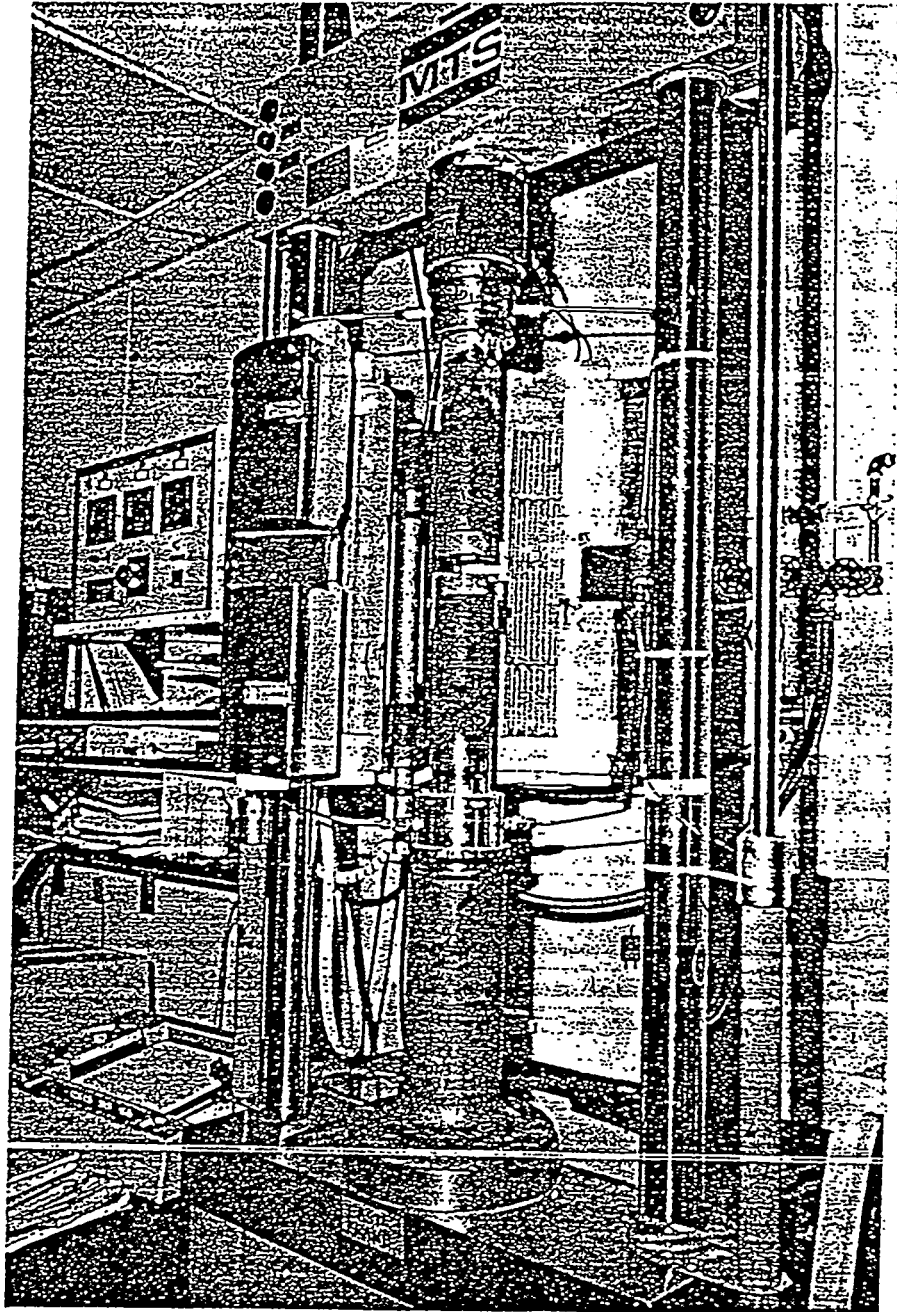


Figure 4 Photograph of hot compression system.

within 5°C during compression.

The test samples were compressed in air at four strain rates (0.001, 0.01, 0.1, and 1 s<sup>-1</sup>), temperatures from the ductile brittle transition to 1000°C, and to a total strain of one ( $\epsilon=1$ ). Test samples were coated with glass, which provided lubrication and protection from surface oxidation, loaded onto the bottom die in the furnace in air, held for 10 min. at the test temperature (specimens required approximately 5 min. to reach the furnace temperature), compressed uniaxially, and quenched in water after deformation.

Compliance in the load train resulted in deviations in  $\epsilon$  and  $\dot{\epsilon}$  up to about -5 pct with the maximum occurring at the lowest temperature, at which the greatest loads were encountered. The true flow stress,  $\sigma$ , can be assumed equal to the true average pressure because the coefficient of friction between sample and die is near zero.<sup>12</sup> In addition the strain distribution can be assumed uniform throughout the specimen and true strain,  $\epsilon$ , can be calculated from the change in test specimen height.<sup>13</sup> Note, for uniform uniaxial compression the effective or significant stress and strain reduce to the axial normal component of stress and strain, as is the case for tensile testing in the uniform elongation realm.<sup>13</sup> Values for  $\sigma$  and  $\epsilon$  were calculated from the as-measured load and corrected displacement data utilizing conventional relationships.<sup>14</sup> Sample dimensions, measured at ambient temperature, were corrected for thermal expansion which occurs on heating to the test temperature. The measured displacement of the sample, obtained with a linear-variable-differential-transformer (LVDT) mounted at the lower end of the moving ram, was corrected for test system compliance. Calculated values of final  $\epsilon$ , obtained from the LVDT displacement and corrected for compliance and for cooling to ambient temperature, were typically within 1 to 2 pct of the measured plastic strain, calculated from the actual initial and final height of the test sample.

### Lubrication

Adequate lubrication is required to provide reliable and consistent data. A review of the effects of friction in compression testing is provided in the ASM book *Workability Testing Techniques*<sup>15</sup>. The general characteristics of frictional effects on the compression of a short cylinder are shown in figure-5. Frictional restraint at the end faces retards the outward motion or diametral expansion of the sample at the faces. This

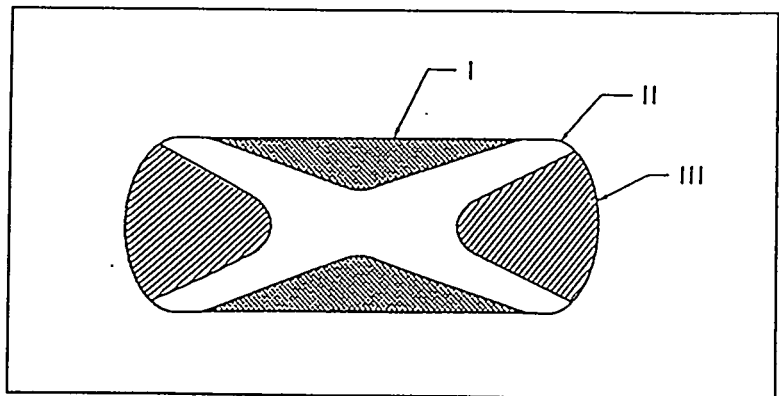


Figure 5 Deformation zones associated with inadequate end lubrication in a cylindrical compression sample

causes the sample to have a greater diameter at the mid-height position, giving it a barreled appearance. At greater strain and continued barreling, material that is originally located on the circumferential surface may rotate enough to eventually contact the die face. Barreling introduces a complex stress state and inhomogeneity in strain and strain rate across the cross section of the specimen. In this case, the as-measured stress does not give a true measure of the material's flow stress.

The inhomogeneity associated with friction and barreling results in three distinct zones of deformation as shown in figure-5. Metal in contact with the compression platens remains stationary, resulting in volumes of material, adjacent to the die face, which are relatively undeformed. These volumes are typically referred to as dead metal zones (region I). The most severe deformation is concentrated in zones of shear just outside the dead metal zones (region II). Metal near the outer surface of the cylinder flows or bulges outward but sees little compressive strain due to barreling (region III). Good lubrication is represented by spreading of the end faces resulting in a straight walled cylinder after deformation with a uniform distribution of strain throughout.

The stress-strain response of a material is most accurately described when ideal lubrication is obtained. Because of this, a significant effort was made to find an appropriate lubricant for each test condition that would result in as close to a uniform state of deformation as possible. Figure 6 shows a beryllium compression specimen before deformation and after deformation to a strain of 1. The straight side walls indicate good lubrication. In this case the original circumferential lip which holds the lubricant on the sliding surface was observed to have spread to the outer most position of the deformed sample face. In some cases, fairly straight side walls have been observed in conjunction with the lack of spreading of the end face. In these instances, the circumferential surface has barreled, come into contact with the compression platens and become part of the end face of the sample, giving the illusion that good lubrication had been attained when in fact it had not.

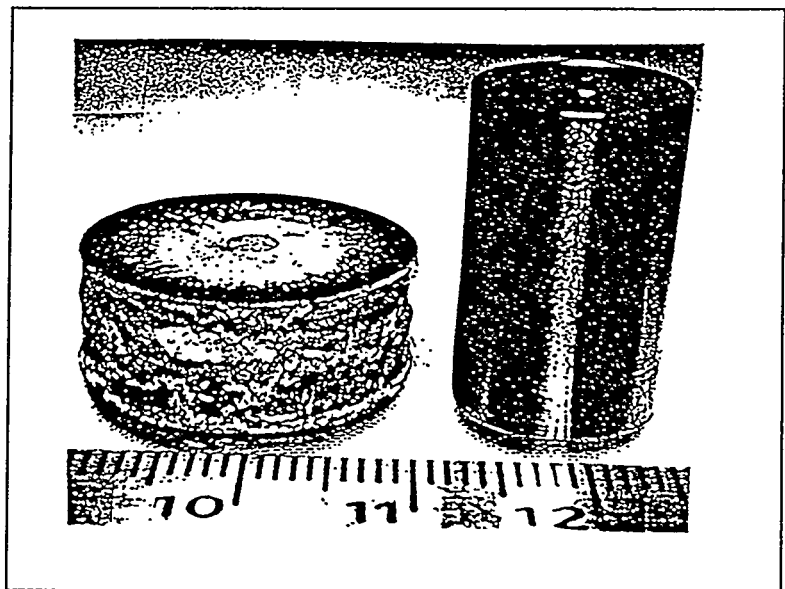


Figure 6 Photograph of a beryllium compression sample before (right) and after (left) testing exhibiting straight side walls and good lubrication. This sample was tested at 600°C and a strain rate of 0.1 s<sup>-1</sup>.

During the lubrication study and subsequent testing, a trend was noticed in the flow curves of test samples that had good and bad lubrication. Figure-7 illustrates the difference found at 700°C and a strain rate of 0.1/s. Curve 1 had excellent lubrication and the flow curve remained relatively flat all the way to the end of the test while Curve 2, which exhibited poor lubrication, not only has a higher flow stress but also turns up at the end. It is believed that the increased flow stress is due to the energy required to overcome friction and the turned up flow curve is a result of the barreled surface coming into contact with the platens which increases the surface area of deformation.

Another trend that was noticed during the testing was the effect of temperature on the apparent lubrication of the specimens. As the test temperature increased general lubrication became worse and more dependent on strain rate. In general, at 400 and 500°C lubrication increased with decreasing strain rate, while at and above 600°C the opposite was true. This may be due to the extremely low flow stress of Be at elevated temperatures compared to the force required to overcome friction.

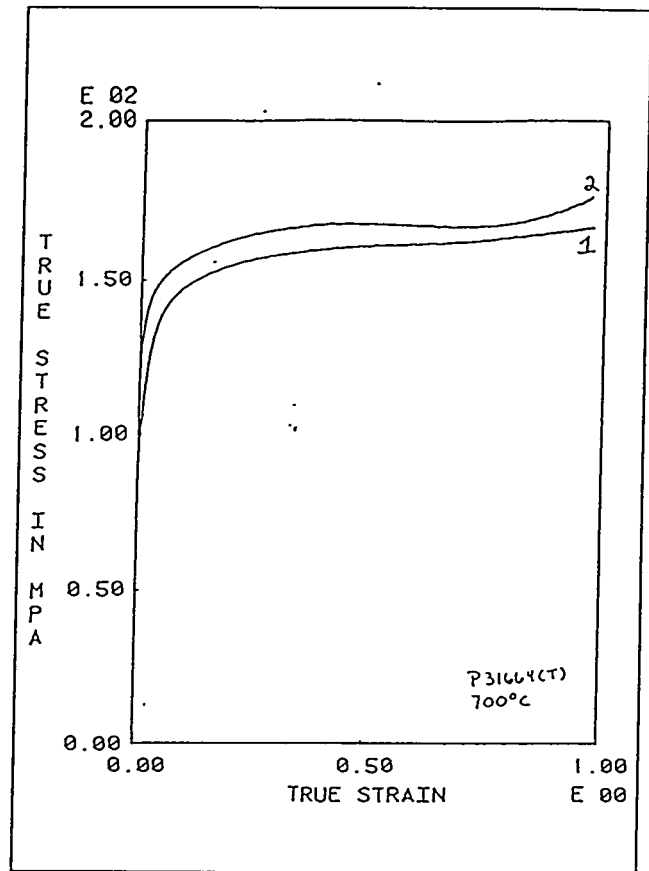


Figure 7 Flow curve comparison between good (curve-1) and poor (curve-2) lubrication. Note the higher flow stress and slope changes associated with the poor lubrication.

## EXPERIMENTAL RESULTS and DISCUSSION

The typical data generated is shown in Figure-7, which gives the stress-strain behavior as a function of strain rate for a specific temperature and material. There are four strain rates shown in each family of curves, 1,0.1,0.01, and 0.001 s<sup>-1</sup>. Note the higher flow stress associated with the higher strain rates and that data is shown as true stress vs true strain. All specimens were deformed to a strain of 1 (64% reduction in height) unless fracture occurred first. The beryllium stress-strain data shows evidence of yield points, serrated flow, strain rate sensitivity, and ductile-brittle transitions. The occurrence and magnitude of these observations will be shown to be dependent on chemistry, texture, and prior thermal history. A metallographic/ microstructural evaluation was conducted on all starting material and, where applicable, powder processing

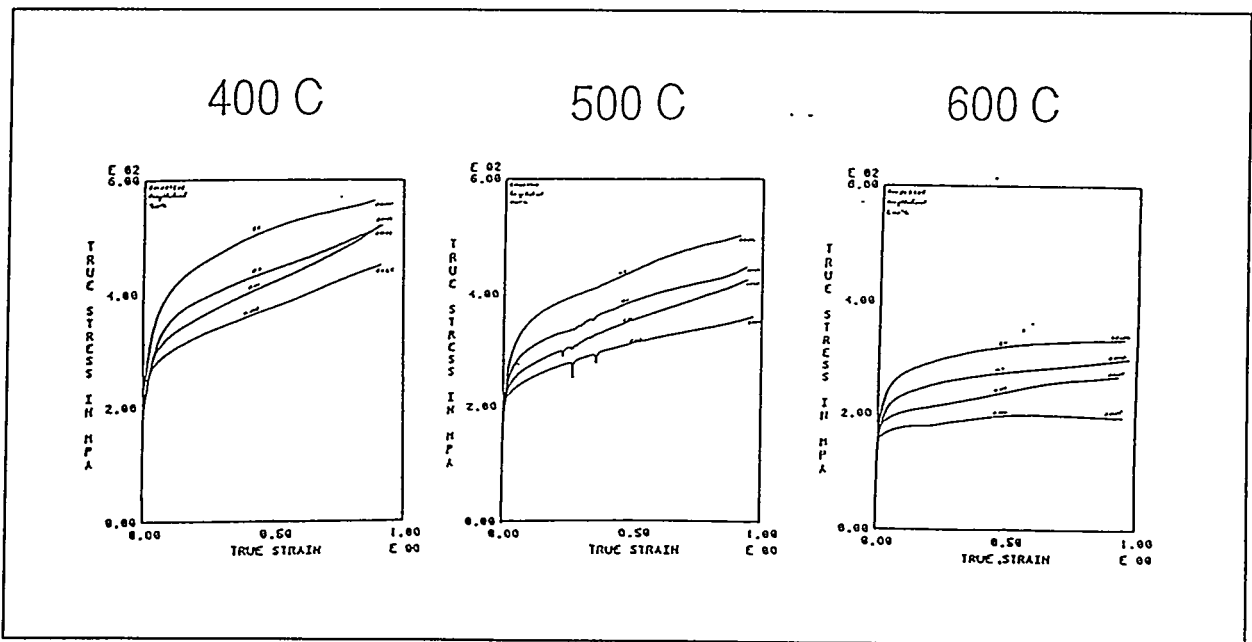


Figure 8 Typical data generated from compression tests showing the stress-strain behavior as a function of strain rate at a constant temperature for RM253939.

history and microstructural characterization is used to rationalize observed properties.

The results and discussion section will be presented as follows:

- Microstructural characterization
- General yield and ductility behavior
- Discrepancies from ideal flow.

The microstructural characterization is discussed first because it supports discussion of

structure/property relationships of the different grades of beryllium. The general yield and ductility behavior then provides an overview of properties and processing requirements to achieve strength and ductility. The discrepancies from ideal flow then point out specific material behavior which can result from processing or service environment.

#### Microstructural characterization

The initial structures of the materials tested were characterized with optical and transmission microscopy. Figures 9-14 show microstructural composites of polarized light and transmission electron photomicrographs of each material tested. Metallographically each material is similar except for the grain size. The grain size in decreasing order is P31664, S200E, RM253939, CIP-HIP-1, I250, and I400. Transmission electron micrographs were taken to reveal the general structure of the matrix and grain boundaries, and delineate any significant microstructural differences which may correlate to property differences.

The P31664 material (figure-9) displayed a relatively low BeO content, with particles generally confined to the grain boundaries and sub-boundaries. Our first examinations showed no significant precipitation of either the  $\text{FeBe}_{11}$  or  $\text{AlFeBe}_4$ . (*didn't really look properly for these in this alloy*) The particles shown residing next to the grain boundaries are oxides. The dislocation density was low.

The S200E material (figure-10) displayed a much higher BeO content, distributed in the grain boundaries and the matrix. It also exhibited a significantly higher dislocation density. Again no precipitates other than oxides were found. (*didn't really look properly for these in this alloy*)

The RM253939 material (figure-11) showed unexpectedly high oxide content in the area examined in the TEM. No significant precipitation of  $\text{FeBe}_{11}$  was observed. A few grain boundary precipitates of  $\text{AlFeBe}_4$  were found, an example of which is shown. The particle was identified as  $\text{AlFeBe}_4$  by EDS and electron diffraction. Some faulting on  $\{111\}$  planes can be seen in the micrograph, consistent with the fcc structure. The dislocation density in this alloy was high, similar to that observed in S200E.

The CIP-HIP-1 material (figure-12) displayed a moderate BeO content, with particles primarily at the grain boundaries and sub-boundaries. The oxide dispersion was very fine, characteristic of hot isostatically pressed material. The grain size was variable, ranging from 3-5mm to over 10mm. The larger grains generally contained sub-boundaries, with relatively high dislocation densities, both in the boundaries themselves and in the surrounding area. Most of the smaller gains were dislocation free.

The I250 material (figure-13) was similar to the CIP-HIP-1, with a moderate BeO content, mostly restricted to the grain boundaries and sub-boundaries. The BeO size and distribution was very fine, characteristic of hot isostatically pressed material. The dislocation density was low.

The I400 material (figure-14) had a very high BeO content. Much of the BeO appears to be sitting on the surfaces of the foil (left standing proud after the matrix was polished away). The BeO is not necessarily associated with the grain boundaries, but appears distributed throughout the microstructure. The dislocation density was low.

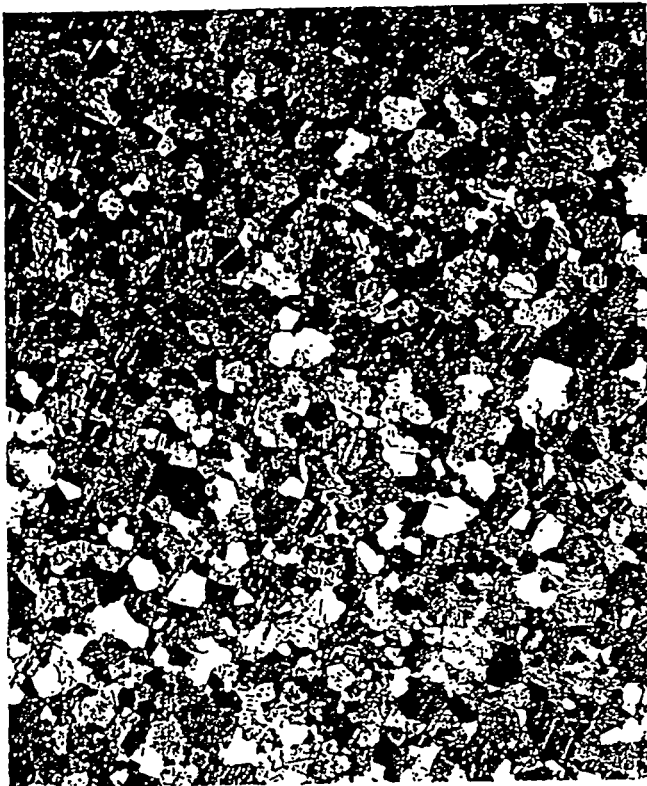
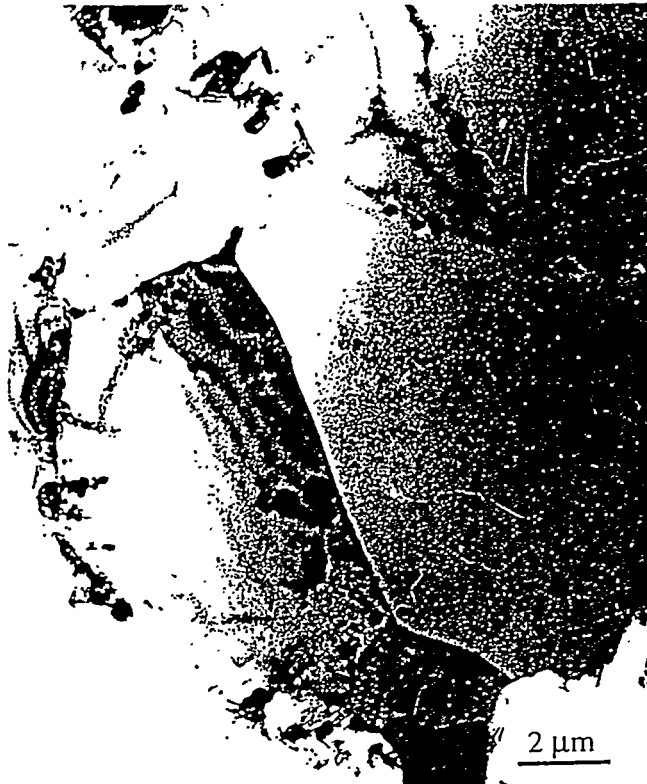


Figure 9 Microstructural composite of P31664 material showing polarized light and TEM photomicrographs.

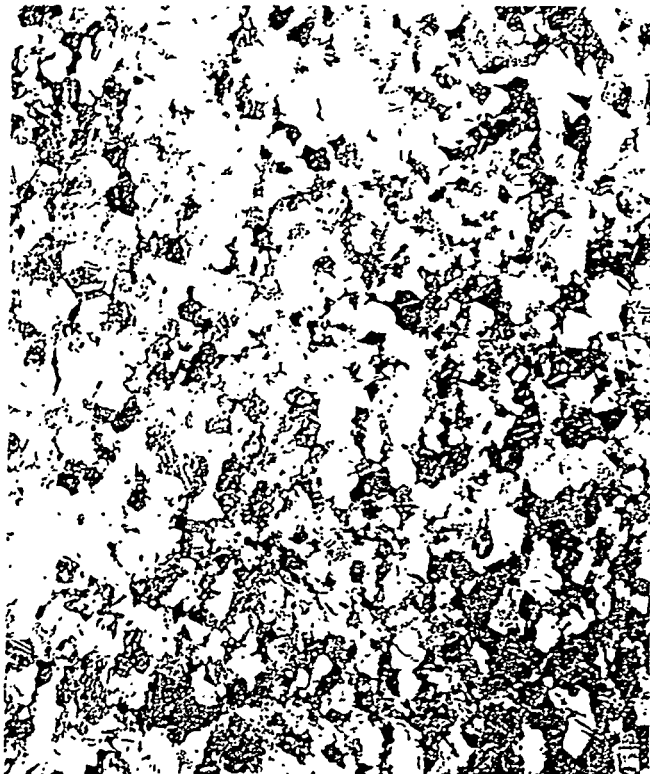


Figure 10 Microstructural composite of S200E material, showing polarized TEM photographs.

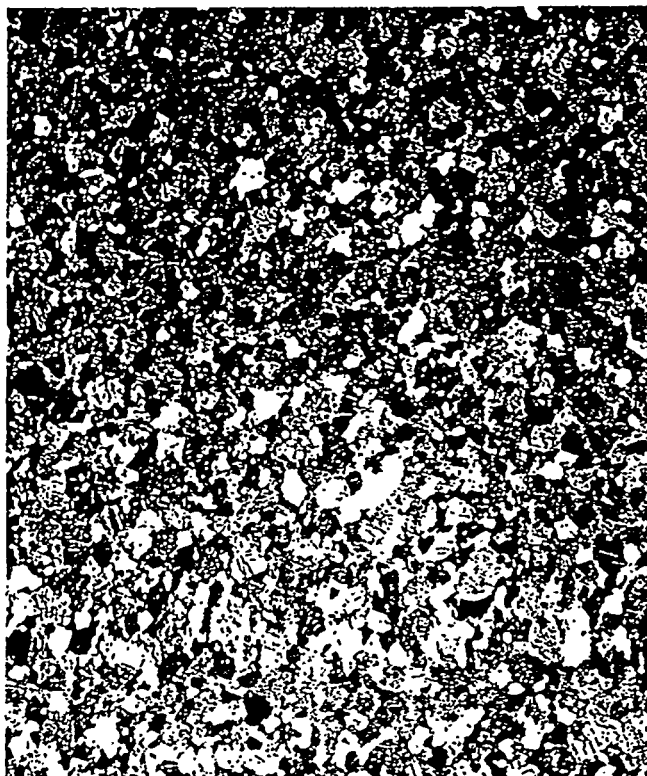


Figure 11 Microstructural composite of RM253939 material showing polarized light and TEM photomicrographs.

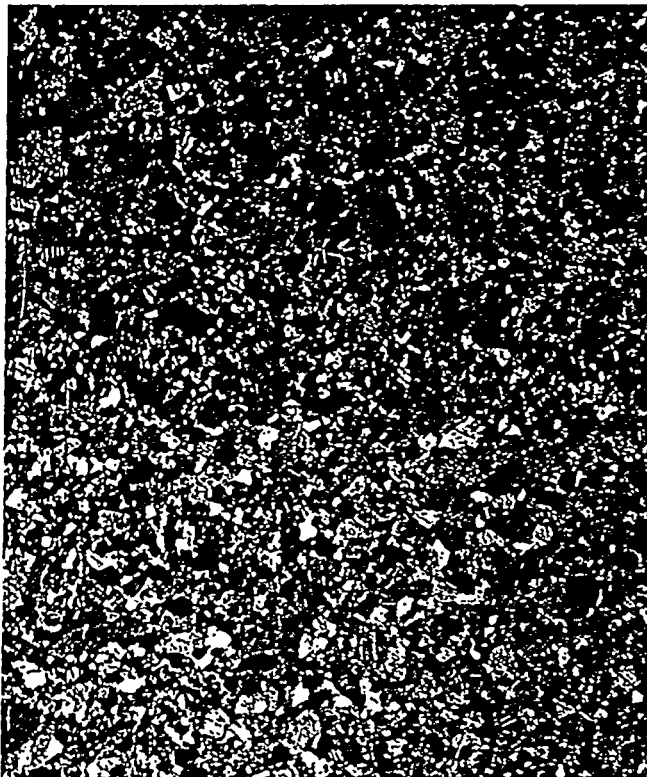
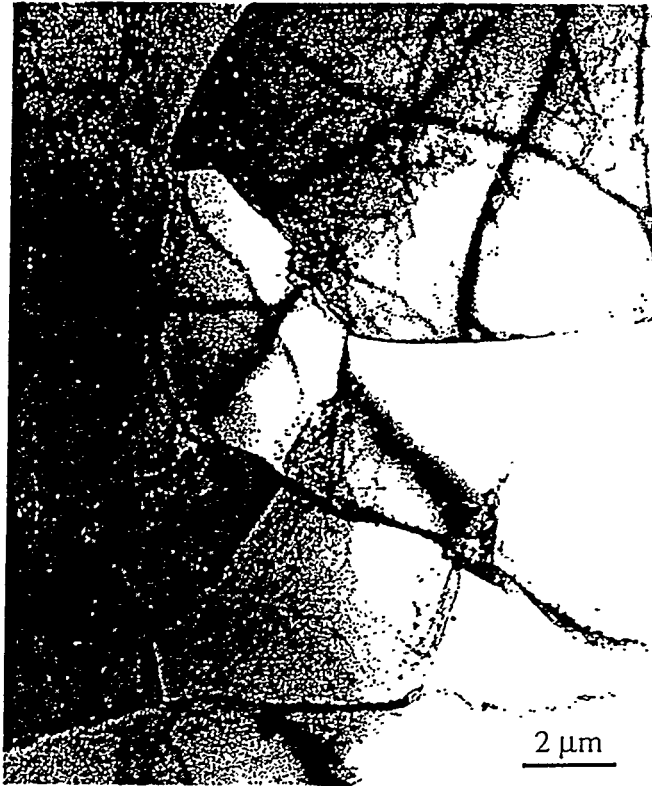


Figure 12 Microstructural composite of CIP-HIP-1 material showing polarized light and TEM photomicrographs.

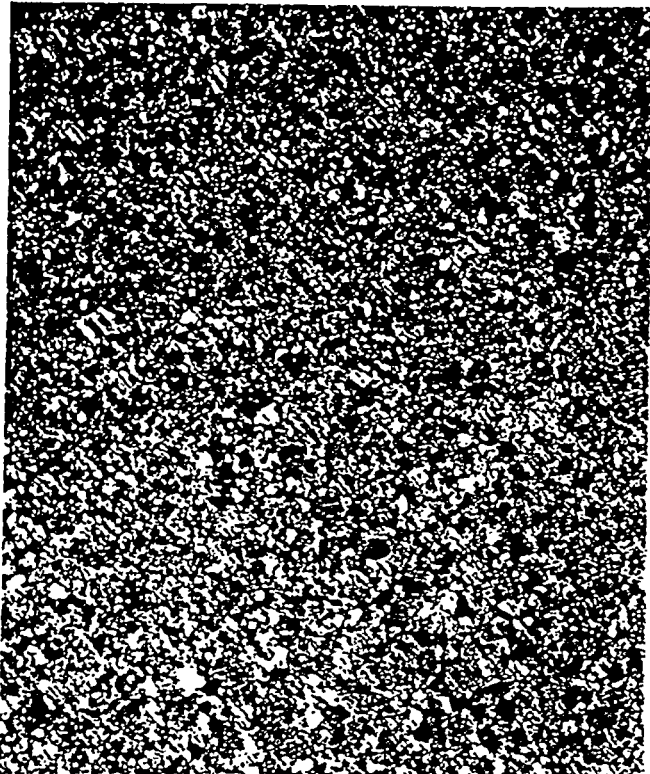


Figure 13 Microstructural composite of I250 material showing polarized light and TEM photomicrographs.

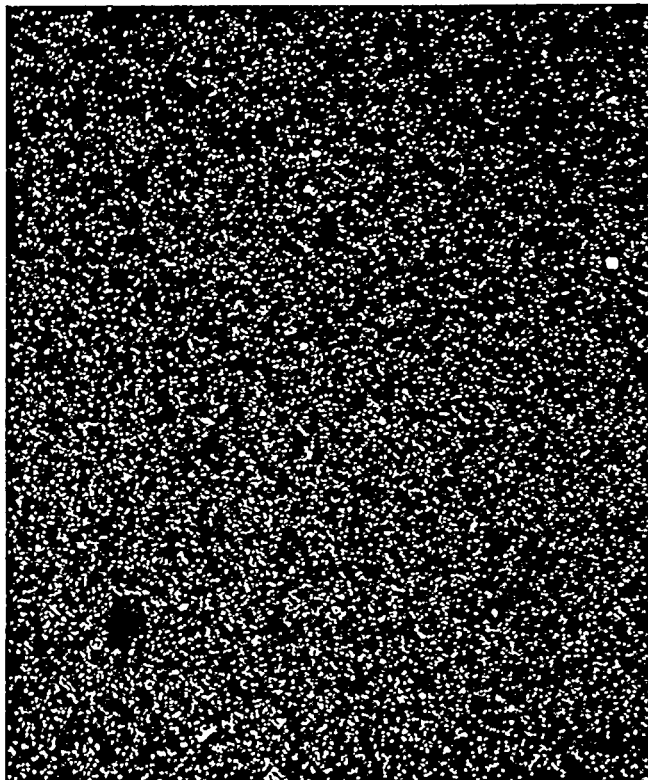


Figure 14 Microstructural composite of I400 material showing polarized light and TEM photomicrographs.

### General Yield and Ductility trends

The 0.2 percent yield strength as a function of test temperature is plotted in Figure-15 for the various alloys compressed at a strain rate of  $0.001 \text{ s}^{-1}$ . From  $25^\circ\text{C}$  to  $900^\circ\text{C}$ , the I400 and I250 alloys are significantly stronger than the other four alloys. In this range, the yield strengths of I400 and I250 are more sensitive to temperature than the yield strengths of the other alloys. As a result, as temperature is increased the yield strengths of these two alloys decrease more rapidly until all of the alloys have about the same strength at approximately  $900^\circ\text{C}$ . Small differences do persist however giving a strength ranking similar to that observed for the alloys at lower temperature.

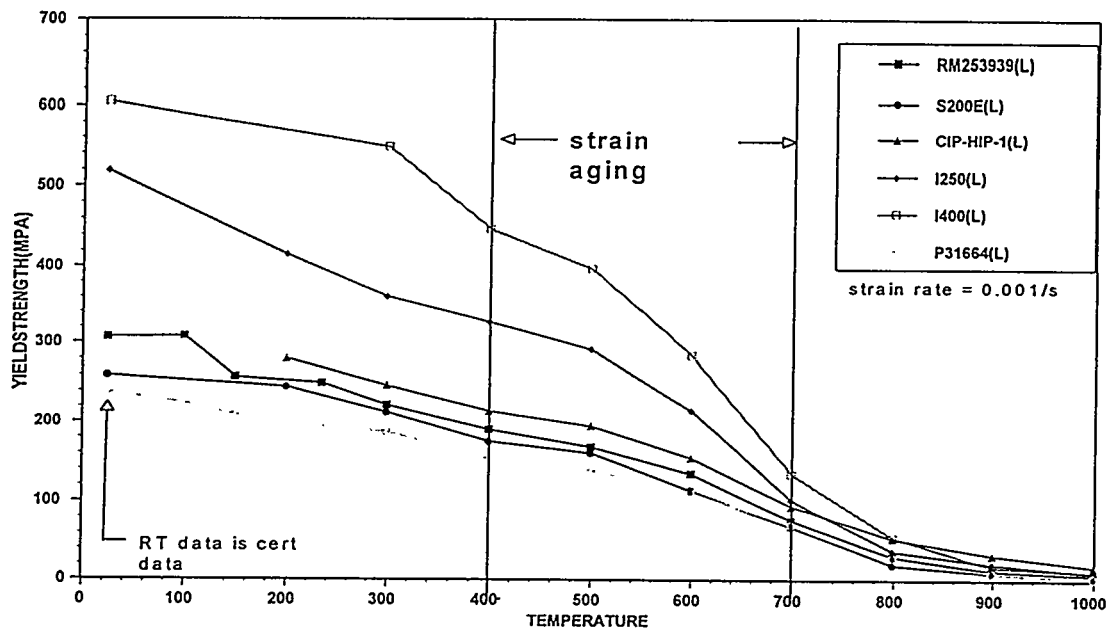


Figure 15 Yield strength as a function of temperature at a constant strain rate of  $0.001 \text{ s}^{-1}$  for all materials tested.

It is interesting to note that the CIP-HIP-1 material yield strength surpasses that of the I250 and I400 at the highest temperatures. This is most likely attributed to the high purity of this alloy. At elevated temperatures free Al and Si at the grain boundaries are molten and would obviously decrease the yield strength. Above  $850^\circ\text{C}$ , even the heat treated material which ties up the Al in the ternary phase, would show dissolution and reduced strengths. Therefore the low microalloy (Al,Si) content of CIP-HIP-1 would account for the improved very high temperature strength.

Figure-15 also shows that all of the strength versus temperature curves show a consistent, small increase at  $500^\circ\text{C}$ , indicating that another strengthening mechanism may be in operation at this temperature. This is also the temperature at which each alloy demonstrated serrated flow curves, or stress-drops, at strains well beyond yielding.

Compression tests were conducted from 1000°C, down to the DBTT, at strain rates of 1 and 0.001 s<sup>-1</sup>. The true strain or reduction in sample height at which failure occurs is plotted as a function of test temperature in Figures 16 & 17 for strain rates 0.001 and 1 s<sup>-1</sup> respectively.

Figure-16 shows that at slow strain rates there is a temperature range of ductile-brittle transition behavior from approximately 400°C down to 100°C depending on the material tested. I400, the strongest material exhibits the highest DBTT. This is followed by a grouping of S200E, CIP-HIP-1, and I250 which show very similar transition temperature. The most ductile materials (showing the lowest DBTT) are the DOE specifications, with the P31664 showing slightly lower DBTT. All materials tested at this strain rate failed from tensile hoop stresses and cracked axially along the compression specimen surface.

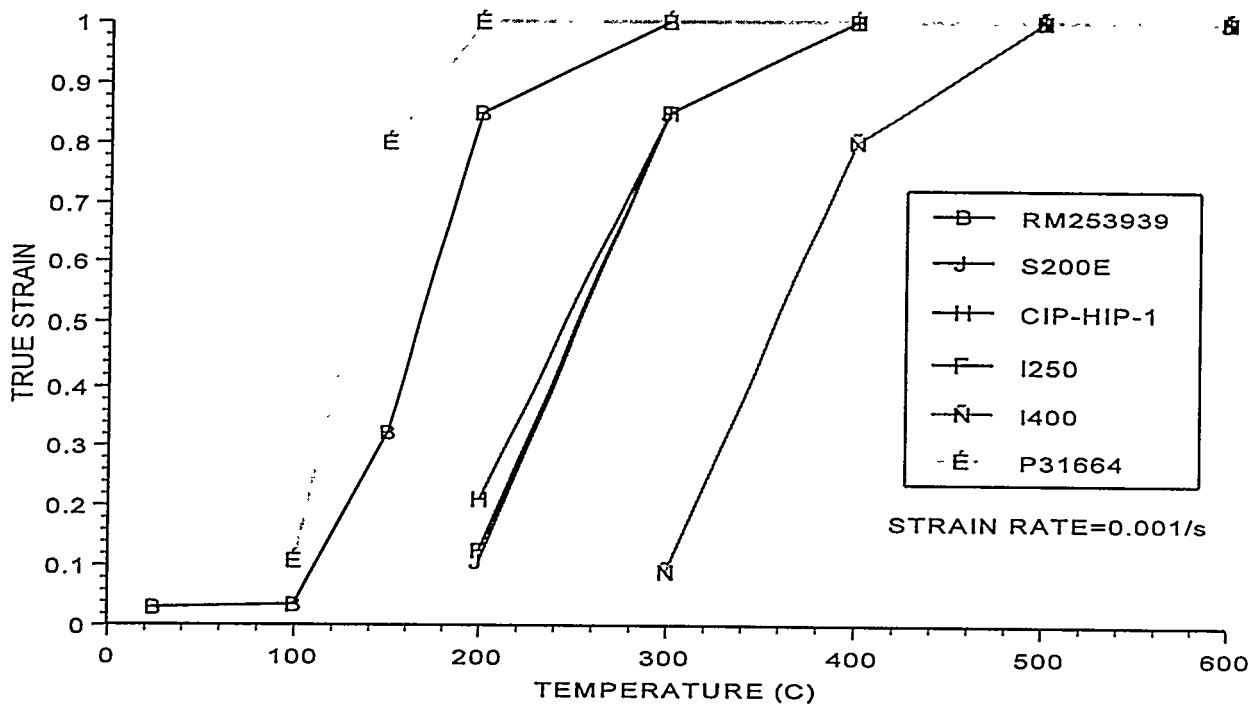


Figure 16 True strain (reduction in height) as a function of temperature at a strain rate of 0.001/s for all materials tested.

It's interesting to note that the materials which show the lowest DBTT's are the two which have been overaged. This results in the precipitation of the ternary compound at the grain boundaries. This compound may blunt cleavage cracks generated in the matrix and prevent their propagation into adjacent grains resulting in improved ductility. Further microstructural investigation is ongoing to better understand this trend.

Figure-17 shows that at the fast strain rate of  $1 \text{ s}^{-1}$  the DBTT range is narrowed to approximately  $200^{\circ}\text{C}$  to  $400^{\circ}\text{C}$ . The data trend is similar to the slow strain rate with the high strength I400 showing the highest DBTT followed by a grouping of alloys S200E, CIP-HIP-1, I250, and P31664, and finally the lowest DBTT is shown by alloy RM253939. The general effect of increasing the strain rate is to shift the DBTT up approximately  $100^{\circ}\text{C}$ . The fracture mode at the higher strain rate also changed from a tensile hoop stress fracture to an adiabatic shear band failure at a  $45^{\circ}$  plane through the specimen. Adiabatic shear bands develop under conditions of high strain rate when the heat generated by local deformation cannot be dissipated. As a result, the local flow stress decreases and further localized flow is stimulated<sup>16</sup>. The fractures are therefore ductile in nature and do not represent true DBTT.

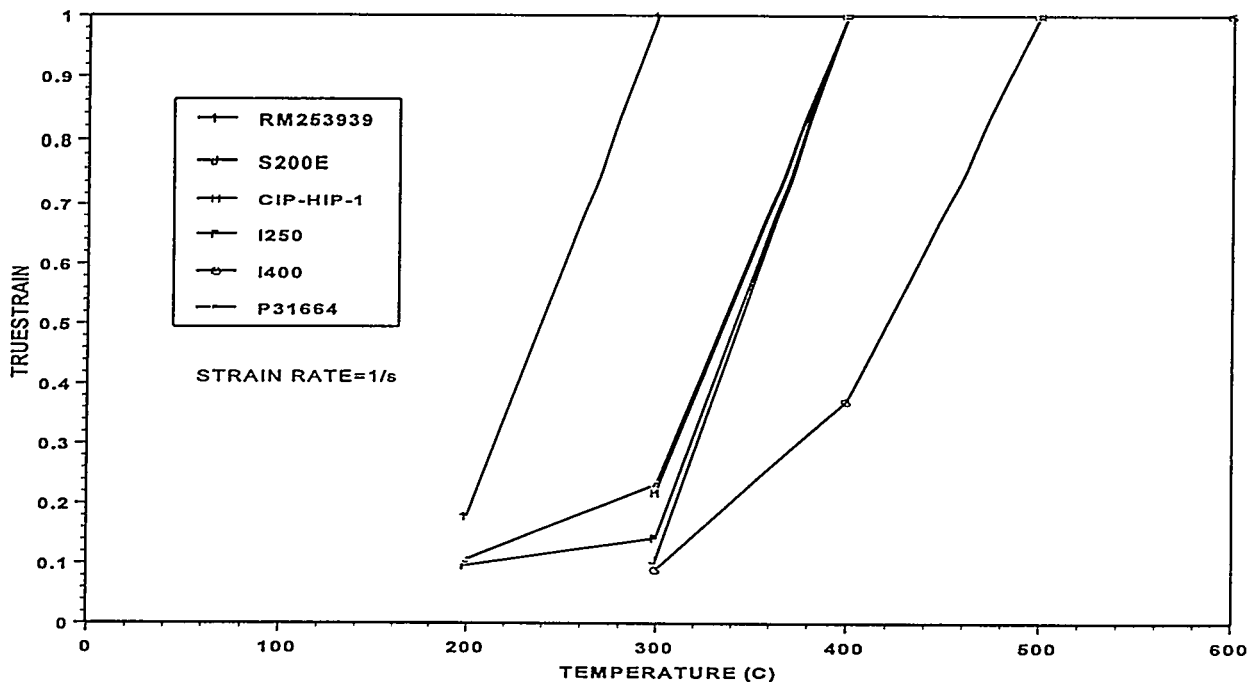


Figure 17 True strain (reduction in height) as a function of temperature at a strain rate of  $1 \text{ s}^{-1}$  for all materials tested.

#### Discrepancies from Ideal Flow

Some of the alloys investigated in this study showed a yield point up to  $500^{\circ}\text{C}$ . Various degrees of yielding were observed and material was noted as having a yield point if there was an inflection or discontinuity in the stress-strain curve at the point of yield, there was a leveling of the flow stress at yield (similar to a Luders' band), or there were the conventional upper and lower yield points. From the DBTT to  $500^{\circ}\text{C}$ , alloys P31664, RM253939, I250, and I400 showed yield points at all strain rates. Alloys S200E and CIP-HIP-1, however, did not exhibit any yield point phenomena. None of the alloys had yield points at or above  $600^{\circ}\text{C}$ .

The number of individual data points used to generate each stress-strain curve is approximately

500 and these are spread evenly over the entire strain range. Therefore the number of data points within the yield point region is limited and only qualitative assessments of the yield point behavior can be made.

Yields points have been observed in many alloys, most notably lightly alloyed alpha-Fe. The yield point, followed by an immediate drop in stress and then usually a period of extensive strain at constant stress known as Luders' elongation has been generally attributed to either of two mechanisms. In the first, dislocations which are pinned by an atmosphere of some impurity or alloying constituent, e.g. C in alpha-Fe, break away from their pinning sites. The avalanche of dislocation movement occurs suddenly and stress drops giving an upper yield point followed by a sharp drop in the flow stress. In the alternate mechanism, existing dislocations are pinned and do not move, but instead at a critical maximum stress, the upper yield point, an avalanche of new dislocations are emitted from sources.

Although yield points and Luders' elongation was not the subject of this study, some interesting observations have been made. In beryllium micro-alloys, it has been shown that slow-cooled and/or aged conditions typically show the yield point phenomenon. During slow cooling and aging treatments, existing dislocations can be pinned by substitutional elements like Fe or precipitates like  $\text{FeBe}_{11}$  and  $\text{FeAlBe}_4$ . Upon reloading, an avalanche of dislocations, by one of the two above mechanisms occurs and an upper and lower yield point is formed. Yield points have been eliminated in beryllium alloys by either heating to high temperature and quenching or by pressurization treatments at relatively low temperature (below the aging temperature range). Either treatment induces new mobile dislocations that are free to move under stress in subsequent room temperature deformation testing. Borch<sup>17</sup> found that the large difference in thermal expansion coefficient with crystallographic orientation should cause large thermal stresses on rapid cooling thereby generating mobile dislocations. In pressurization treatments, new dislocations are also thought to be introduced. Once eliminated by these type of treatments, yield points can be reintroduced by heating into the precipitation range and/or by slow cooling from a high temperature allowing either precipitation or solute atom pinning of the dislocations.

Consistent with the results in the literature, the three materials in this study which demonstrate the yield point phenomena are ones which were given either a stress-relief or an over aging heat treatment. Both of the treatments involve time at temperature for diffusion of Fe to dislocations or precipitate formation on dislocations. These materials are the P31664 and RM253939 alloys, which were overaged, and I250, which was stress relieved. The two other materials which were not given any post-consolidation heat treatment, S200E and CIP-HIP-1, demonstrated a smooth flow curve in the low strain region with no evidence of the yield point phenomena.

The behavior of I400 appears to be an exception to the above results because it was not heat treated but does have a yield point. It could be that cooling after consolidation was slow enough in this particular heat that dislocation pinning was fostered or that the Fe content, which is much higher in this alloy than the others, results in the rapid pinning of dislocations on cooling. The production histories of all of the alloys are being further investigated in the ongoing study for

more detail on the cooling and post heating cycles in order to shed light on the origin of the yield point phenomena.

Serrated flow was observed in all materials tested. A follow on study will attempt to model these observations as a means of identifying the operable mechanism. Their presentation here is aimed at raising awareness in relation to the operating environment in ITER and proposing probable mechanisms.

The general characteristics of the serrated flow are shown in figure-18. These type serrations were only observed at 500°C, which is within the operating range for Be plasma facing in ITER. The serrations are peculiar in that the curves generally do not oscillate in stress about a mean value, thus exhibiting upper and lower yield points, but instead serrations are composed solely of intermittent stress-drops. The character of the stress-drops varies with strain rate.

Generally, as strain rate is lowered from 1 to  $.001 \text{ s}^{-1}$  the magnitude of the stress-drops increase while their frequency decreases.

Undulations in the flow stress which occur at strains which are well past the yield strain have been referred to as discontinuous yielding, serrated yielding, or jerky flow, and have been attributed largely to dynamic strain aging. During dynamic strain aging, moving dislocations have a velocity which is similar to the diffusing solute. Dislocations become pinned by the solute and then become mobile again after

considerable increase in stress. Stress rises due to pinning and falls upon unpinning. For the effect to be observed as a macroscopic effect on the flow curve, large numbers of dislocations must undergo pinning and release at the same time. This phenomenon is affected by strain rate and temperature. For example, as strain rate increases, the dislocation velocity becomes much greater than the diffusing solute atoms and pinning does not occur. At lower temperatures, the velocity of the diffusing species is retarded, eliminating pinning. At high temperature, the

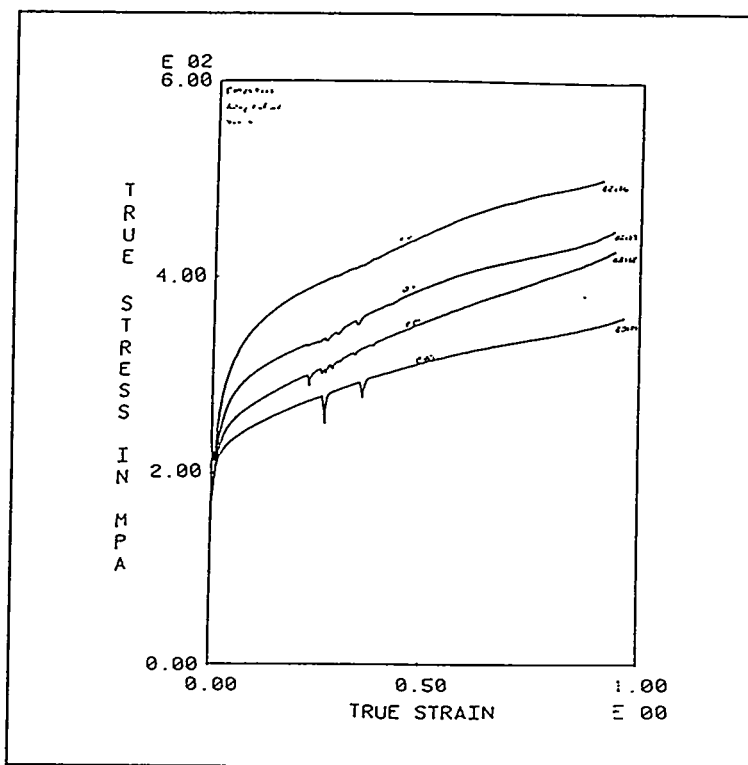


Figure 18 General characteristics of serrated flow observed at 500°C. The material shown is RM253939 at strain rates of 1, 0.1, 0.01, and 0.001.

velocity of the pinning species may be fast enough so that the dislocations never break away, but instead the solute exerts a constant drag on the dislocations, and again unpinning may not occur.

In this study, serrated flow was observed in each alloy at a deformation temperature of 500°C. The effect was minimized by increasing strain rate which is consistent with dynamic strain aging. The observed increase in frequency and decrease in amplitude with increasing strain rate may also be consistent with dynamic strain aging, but remains unexplained at this time. Also consistent with typical dynamic strain aging, the serrated flow disappears as temperature is lowered or raised. No serrations were observed in any of the alloys at 400°C, and only occasional small serrations were observed at 600°C. Another interesting aspect of the serrations is that in most of the alloys tested at 500°C, only two major stress drops, serrations, were observed at the lowest strain rate.

Serrated yielding was reported by Gelles and Peterson<sup>(9)</sup> to occur during tension testing at 476°C and at a strain rate of 0.00064 s<sup>-1</sup> for various grades of hot-pressed block (HP-10 and HP-21 from KBI, and S-240 from Brush, Inc.). The serrations generally occurred in the strain range between 0.03 and 0.15, and damped out before tensile specimen failure. This strain range is well below that observed for serrated yielding during compression. In this study, testing at similar temperature and strain rate, 500°C and 0.001 s<sup>-1</sup>, showed the strain range to vary from about 0.15 to 0.5. This difference in the critical strain for serration nucleation between tension and compression indicates that the mechanism for serrated yielding is inhibited by compression. In general, the fluctuation in the magnitude of the flow stress is much greater while the frequency of serrations is much smaller in compression compared to tension, from qualitative observation of the published tensile curves<sup>(9)</sup>. These observations also appear to be consistent with the above suggestion that compression inhibits serrated yielding. For example, a large potential for the first stress drop may accumulate during the relatively large pre-straining period in compression, with the critical strain ranging from 0.15 to 0.3 in compression versus 0.03 to 0.05 in tension. The large accumulation of strain may then be expected to result in a large stress-drop followed by another period of serration-free flow before a subsequent stress-drop occurs. In tension, serrated flow appears to be unrestricted, starting at a low critical strain and progressing in small bursts at high frequency.

In both tension and compression, serrations were peculiar to the temperatures near 500°C. Tension testing at 370°C and 595°C and compression testing at 400°C and 600°C did not produce serrated yielding, although minor serrations did occur in compression at 600°C in the S200E, I250, and I400 materials.

One notable exception to the general agreement between the tensile study<sup>(9)</sup> and this study featuring compression testing was that the results on the same grade of beryllium, S200E, do not agree. Serrated yielding was not observed in tension while large stress-drops, relative to the magnitude of the stress drops observed for the other materials in this work, were observed in compression. The reason for this discrepancy can not be explained at this time. It has been suggested by Weisz et al<sup>10</sup> that a critical strain for serrated flow, assuming a dynamic strain aging

mechanism, is related to the achievement of a critical vacancy density which enhances diffusion of the pinning species to a level that the species can move effectively to pin the mobile dislocations. Considering this, one would expect that at higher strain rates, the critical vacancy density would be achieved at a lower measured strain because at the higher rate there would be less time for dynamic annealing of the vacancies as they form. In this case, a reduction in the critical strain should occur with increased strain rate as was generally observed for the materials tested in this study, except for I400. The average velocity of the dislocations would increase with strain rate, but may be moderated by an increase in dislocation density. The role of dislocation velocity and density, and their potential effects on the nature of serrated yielding is beyond the scope of this report and is not considered further.

## CONCLUSIONS

In general, the flow curves at high strain rates showed work hardening at the lowest temperatures and work softening at the highest temperatures. HIP'ed material generally showed less work softening. At low strain rates, work hardening was observed at low temperatures. At high temperatures, the flow stress typically achieved a steady state. Between 25 and 700°C and at the strain rate of 0.001 s<sup>-1</sup> the ranking of the yield stress between materials is consistent. The materials are listed in descending order of strength: I400, I250, CIP-HIP-1, RM253939, S200E, P31664. At 900 and 1000°C CIP-HIP-1 material has the greatest yield strength, followed by I250.

Serrated flow was observed in all the materials tested and was most pronounced at 500°C, showing large drops in the flow stress. Three common factors among all materials tested were:

- serrated flow was not observed until a critical amount of strain was accumulated;
- the magnitude and occurrence of the serrations was strain rate dependent showing greater magnitude serrations at the slowest strain rates and almost complete elimination at the high strain rates;
- serrated flow was only observed within a specific temperature range. Sharp, large serrations were observed at 500°C and minor perturbations in the flow stress up to 700°C.

One material was tested in the transverse direction. Serrations were more pronounced when the test sample axis corresponded to the longitudinal axis of the starting billet material.

Trends in the data related to the observance of yield points were as follows:

- no yield points were observed above 600°C;
- the yield points became more pronounced at higher strain rates when tested at 500°C;
- the yield points became less pronounced at higher strain rates when tested at 400°C;
- both the S200E and CIP-HIP-1 materials did not exhibit yield points.

Strain rate sensitivity was observed in all alloys showing a greater difference in yield and flow stress as temperature was increased. The higher strain rate showed the greater yield and flow stress.

## RECOMMENDATIONS

- 1) Building block material Al/Fe ratio should be controlled and material heat treated to control hot shortness and improve ductility.
- 2) Aluminum content of plasma spray material should be minimized (<200ppm) to minimize hot shortness.
- 3) Consideration should be given to writing specifications for ITER applications.
- 4) ITER Be material should be designed for resistance to thermal fatigue and not based on yield strength data.

REFERENCES:

- 1)I.I. Papirov and G.F. Tihinskiy, Structure and mechanical properties of fine-grain deformed beryllium, Phys. Metals Met., (English translation of Fiz. Metal. Metalloved>), 29(5), 167-169, Pergamon Press, London (1971).
- 2)D. Webster, The effect of low melting phases on the elevated microstructural stability of hot pressed beryllium, Met. Trans. 6A, 803-808 (1975).
- 3)A.J. Stonehouse, Beryllium science and technology Vol I,pp200-201, Plenum Press, New York and London.
- 4)R.A. Foos, A.J. Stonehouse, K.A. Walsh, Microalloying Relationships in Beryllium, Brush Wellman Report BBC-TR-456, March 23, 1970.
- 5)A.B. Brown, F. Morrow, A.J. Martin, An improvement in the ductility of beryllium at high temperatures, Nature 187, 494-496(1960).
- 6)S.M. Myers, J.E. Smugeresky, Phase Equilibrium in the Be-Al-Fe System Using High Energy Ion Beams, Met Trans 7A, 795-802(1976)
- 7)D.R. Floyd, Causes of Yield Point Phenomenon in Commercial Beryllium Products, Feb. 1,1974, Rocky Flats Plant Report RFP-2061.
- 8)A.B. Brown, F Morrow, A.J. Martin, The effect of strain rate, and heat treatment, on the tensile properties of extruded beryllium rods between 25 and 600°C, J. of Less Common Metals, 3,(1961) 62-88.
- 9)S.H. Gelles, J.H. Peterson, Characteristics of Commercial Vacuum-Hot-Pressed Beryllium, BMI-X-629, Sept. 1972.
- 10)M. Weisz, J. Mallen, Y. Adda, Study of the portevin Lechatelier Effect in Berylliu of Commercial Purity, Sixth Metallurgy Colloquim of Scalay, July 1962, University Press (1963).
- 11)G.J. London et al, Grain Size and Oxide Content affect Beryllium's Properties, Metals Eng. Quart.(August, 1976)
- 12)G.W. An introduction to the Principls of Metalworking, Edward Arnold, London, 1965, p.245.
- 13)G.E. Dieter, Mechanical Metallurgy, 2nd ed., McGraw-Hill inc., New York, NY, 1976, pp72-102.

14)M.C. Mataya, V.E. Sackschewsky, Effect of Internal Heating During Hot Compression on the stress-strain Behavior of Alloy 304L, to be published in Met. Trans.

15)Workability Testing Techniques, American Society For Metals (1984).

16)H.C. Rogers, Ann. Rev. Mater. Sci., 1979, vol.9, pp283-311.

17)R.W. Armstrong, N.R. Borch, Thermal Microstresses in Beryllium and other HCP Metals, Met. Trans. 2, 3070-3077 (1971).